Nuclear Materials and Energy 22 (2020) 100717

Contents lists available at ScienceDirect

Nuclear Materials and Energy

journal homepage: www.elsevier.com/locate/nme

Cavity formation and hardness change in He implanted EUROFER97 and EU-ODS EUROFER

M. Roldán[a,*], P. Fernández[a], J. Rams[b], A. Gómez-Herrero[c], M. Malo[a]

[a] Division of Fusion Technologies, National Fusion Laboratory, CIEMAT. Avenida Complutense, 40. Madrid, Spain
[b] Department of Applied Mathematics, Materials Science and Engineering and Electronic Technology, School of Experimental Sciences and Technology, Rey Juan Carlos University, C/ Tulipán s/n, Móstoles, Spain
[c] Centro Nacional de Microscopía, Universidad Complutense de Madrid. Avenida Complutense, S/N, Madrid, Spain

ABSTRACT

RAFM steels EUROFER97 and EU-ODS EUROFER samples have been implanted with He ions at 40 keV (ion penetration depth ~300 nm) at a dose of ~ 1×10^{15} ion/cm^2 and different temperatures up to 550 °C.

Post-irradiation examination of the samples has been performed using nanoindentation along with conventional and scanning transmission electron microscopy (CTEM/STEM in Annular Dark Field mode). The specimens were indented up to 500 nm by CSM method (Continuous Stiffness Measurement), in order to assess the changes in nanoindentation hardness values due to the irradiation. After indentation tests, lamella was extracted from each implanted sample which included at least one nanoindentation cross-section. The changes in hardness were correlated with any microstructure modification detected by TEM. A clear trend can be observed; the hardness values increased with irradiation temperature, as well as the He bubble nucleation and population density. A remarkable change in bubble distribution in EUROFER97 was found at the two highest irradiation temperatures (450 °C and 550 °C). In contrast, an increase in the cavities size was observed in EU-ODS EUROFER, but no new nucleation was observed for the same temperatures. These observations suggest that for these particular conditions, the cavity growth is enhanced, rather than new nucleation, which depends strongly on the material microstructure.

1. Introduction

The materials which will be part of the future nuclear reactors will have to withstand high temperatures (250 – 550 °C/650 °C), time-varying stresses and neutron irradiation during their whole service life [1–5]. It is well known that irradiation causes an essential degradation of the structural materials, and the design of the future fusion reactor requires that both microstructural and mechanical properties are examined under such a severe environment, or at least as closerly as possible.

EUROFER97 and EU-ODS EUROFER (which refers to ODS-EUROFER European batch produced by Plansee [6] available to different European Laboratories such as CIEMAT) reduced activation ferritic-martensitic (RAFM) steels are candidates to be used as structural materials due to their reduced activation, good corrosion resistance and especially their low He and H transmutation ratio under neutron irradiation [1]. In addition, Oxide Dispersion Strengthened (ODS) steels are one of the most promising material families for nuclear fusion application [7], since they may accommodate the defects generated during irradiation due to their characteristic microstructure. These materials have an improved irradiation resistance, especially at very high temperatures (which may enhance thermodynamic cycle increasing the upper operating temperature by 100 °C to 200 °C [8]) because of the high amount of defect sinks within their own microstructure in form of Yttria particles and high dislocation density dispersed along the matrix in comparison with typical non-ODS steels [1,5,9–11].

Neutron irradiation not only will cause high radiation damage (~50 dpa) producing hardening and high density of nanoscale defect clusters (dislocation loops and cavities) which serve as obstacles to dislocation motion [4,12] but also He and H generation as transmutation products within the material, which will lead to modifications of the original microstructure generating cavities, affecting the mechanical and physical properties [8,13]. It is expected that upon completion of the whole reactor service life around 700 – 900 appm He will generate inside the structural materials [1,14,15].

In the last 50 years, abundant scientific research has been conducted with the objective of gaining insight into the He bubbles nucleation and development mechanisms. He is practically indissoluble in metals, and it tends to migrate and create bubbles or voids (generally referred to as cavities since that term encompasses voids and bubbles as irradiation defects [16]) whose size, density, internal pressure or nucleation sites, depending on parameters such as the way to introduce (or generate) He into the material, its microstructure, irradiation temperature, projectile energy, final atomic concentration and displacement damage (dose and dpa) and dose rate (flux) [13,17].

* Corresponding author.
E-mail address: marcelo.roldan@ciemat.es (M. Roldán).

https://doi.org/10.1016/j.nme.2019.100717
Received 13 June 2019; Received in revised form 4 November 2019; Accepted 16 November 2019
Available online 20 November 2019

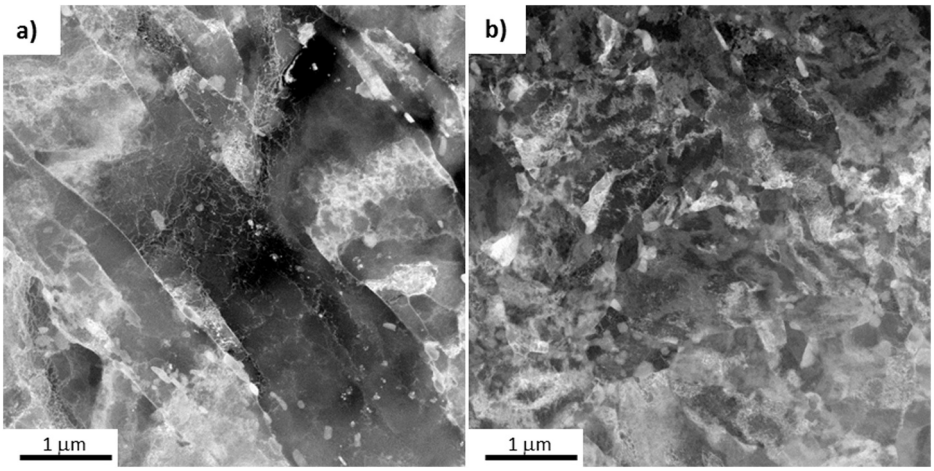

Fig. 1. ADF - STEM micrographs showing the microstructure of (a) EUROFER97and (b) EU-ODS EUROFER in the as-received state (normalized and tempered).

The aim of the present work is to assess the effect between He implantation, irradiation temperature (RT, 350 °C, 450 °C and 550 °C) and the interaction with different microstructural characteristics (such as microstructural phases or dispersed oxides) on EUROFER97 and EU-ODS EUROFER steels. In order to achieve this, nanoindentation by means of CSM module and S/TEM modes were used to analyze and to correlate the hardness response with the microstructural features due to He implantation.

2. Experimental procedure

2.1. Materials

The materials investigated in this research were the reduced activation ferritic/martensitic steels denominated EUROFER97 and EU-ODS EUROFER (Fig. 1a - b). Both alloys have the identical chemical composition (wt.%): 0.11C, 8.7Cr, 1 W, 0.10Ta, 0.19 V, 0.44Mn, 0.004S, balance Fe. The EU-ODS EUROFER also contains 0.3 wt.% of Y_2O_3 particles. Those particles have been extensively studied by Ceri A. Williams et al. [18] where it was demonstrated that they were formed by an Yttrium-rich core surrounded by Cr and V rich shell. Regarding microstructural features, EU-ODS EUROFER has a ferritic matrix with an average value of grain size of 0.98 ± 0.48 µm (measured by EBSD with no clear texture detected [19]). However, it is possible to find grains between 0.5 and 4 µm, which means that this alloy has a very heterogeneous grain size. The average Yttria particles size added to the matrix was 20 nm, but their distribution was not very homogeneous, finding both small clusters of them and large areas with no particles within the matrix. In the case of EUROFER97, the matrix is fully martensitic, its primary austenite grain size is between 6.7 and 11 µm and the average size of martensite laths is between 0.3 and 0.7 µm, with equiaxed morphology. In contrast to EU-ODS EUROFER since it has ferritic tangle grains, as shown in Fig. 1b). The steels have been studied in the normalized (980 °C/27 min air-cooled) plus tempered (760 °C/90 min air-cooled) condition for EUROFER97 (Heat E83698) and normalized (1150 °C/60 min air-cooled) plus tempered (750 °C/120 min air-cooled) for EU-ODS-EUROFER (Heat HXXX1115), denominated in this paper as the as-received state. Detailed chemical composition, microstructural characteristics and mechanical properties for both materials are given elsewhere [20–22]. EUROFER97 was fabricated using raw materials selection (no scrap) and appropriate clean steel, making technologies to get such a specific composition. It was melted under vacuum induction furnace (VIF) and manufactured following continuous casting. EU-ODS EUROFER, instead, was produced by powder metallurgy. Firstly, the steel was fabricated and atomized under an inert atmosphere. After the process of mechanical alloying of the powder, its consolidation was mainly done by hot isostatic pressing (HIP)

The steel samples were 3 mm diameter discs prepared by mechanical thinning up to 100 µm and finally punched out. Afterwards, each disc surface was polished mechanically up to colloidal silica OP-S with a particle size of 0.04 µm before implantation, since it is required to have a defect-free surface to avoid any artefact for nanoindentation tests.

2.2. Irradiation

Irradiations were carried out with a Danfysik 60 kV ion implanter at the National Fusion Laboratory (CIEMAT). A special sample holder was used for these irradiations, which permitted simultaneous irradiation of four small samples.

In each irradiation, two discs for nanoindentation and TEM of EUROFER97 and EU-ODS EUROFER were introduced into the accelerator chamber to be implanted with He ions at 40 KeV at four different temperatures: RT, 350 °C, 450 °C and 550 °C, with a fluence of 9.5×10^{14} He ions cm^{-2}. The irradiation was carried out with a uniform ion beam (~10 mm diameter). For these measurements, the current intensity stability has been maintained with variations up to 30%, which has been considered tolerable given the purpose of the experiment, which in this case is the implantation of a fixed-dose. Due to the ion current variations mentioned above, the dose rate slightly varies: 0.4 appm He/s (RT), 0.42 appm He/s (350 °C), 0.71 appm He/s (450 °C) and 0.55 appm He/s (550 °C).

MARLOWE code [23,24] was employed to simulate He damage profile, as shown in Fig. 2. The selected energy and dose produced a damage peak, in terms of dpa, with a value around to 0.2 dpa, located between 100 nm and 150 nm depth, with a maximum concentration of approximately 800 appm He. MARLOWE code is more realistic than the SRIM code since the materials simulated are crystalline.

2.3. Nanoindentation tests

The nanoindentations were performed with an MTS Nano Indenter XP equipped with a Berkovich diamond indenter tip (Fig. 3) whose status was checked at the beginning of this research in order to analyze possible roundness or another quality issue [25,26]. Continuous stiffness measurement mode (CSM) method was used to determine hardness values. This method has a resolution in depth of nanometers [27] through the normal surface to irradiation, as can be seen in Fig. 4. This is the most suitable method to detect any hardness variation when a shallow damage volume is analyzed, as seen here where there is a depth of 300 nm, accordingly with Fig. 2. This way, it is possible to evaluate the potential changes of hardness values as the helium concentration

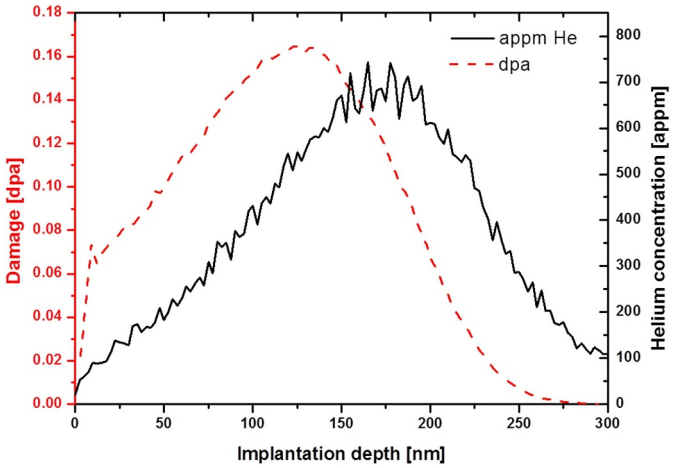

Fig. 2. He concentration and dpa profile produced due to the implantation of He at 40 keV calculated by means of MARLOWE with a fluence of 9.5 × 10^{14} ions/cm^2.

varies with depth, locating the maximum at 150–175 nm approximately according to the aforementioned simulation.

Different indentation matrixes distributed all along the surface of the implanted discs were performed, far enough from the disc edge in order to avoid possible beam shadowing (the very perimeter of the discs were covered by the sample holder, so the beam did not fall upon the samples).

2.4. Transmission electron microscopy

Lamellae from each disc irradiated at every temperature (RT, 350 °C, 450 °C and 550 °C) were extracted using ex-situ lift-out procedure [28,29] with a double beam Ga-ion and field emission electron microscope (FIB-FESEM) by Zeiss with a Ga acceleration voltage between 30 kV to 1 kV. Low Ga ion kV was used to perform a final polishing process in order to remove as much of the Ga induced damage as possible [30,31]. In addition, the volume affected by indentation was studied extracting lamellas containing indentation cross-section Fig. 5 (a–c). Afterwards, those specimens were thoroughly studied by transmission electron microscopy using a TEM JEOL 2100HT at 200 kV and a STEM JEOL 3000F at 300 kV. In some particular cases, new JEOL STEM ARM 300 kV was used to check the structure more in detail. Cavities were characterized by the through-focus bright field sequence method [32,33] with the specimen tilted away from the Bragg condition, in order to minimize the orientation contrast which may complicate the identification of cavities. The thickness of each lamella window to calculate the characteristic parameters was obtained using CBED diffraction pattern, as it was successfully done and published in [32]. Thickness lamella values vary between 78 and 105 nm because it strongly depends on the effective ion current at every experiment, which is critical at the final stages. Measurements of the cavity

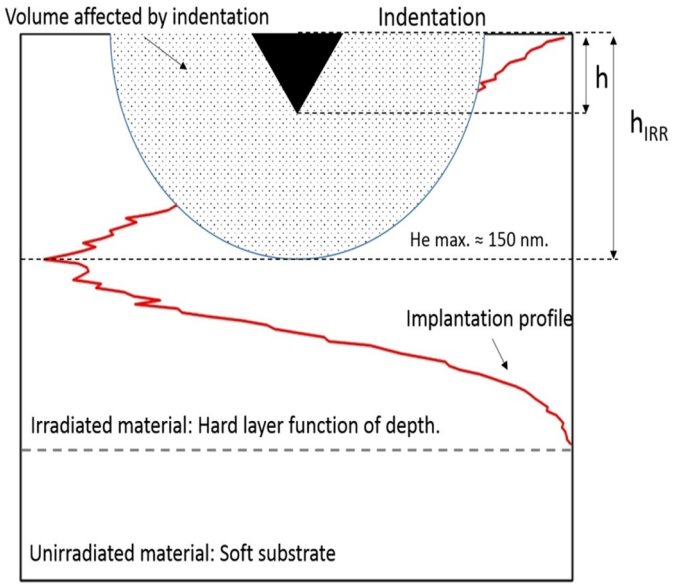

Fig. 4. Scheme showing the interaction between the volume affected by the indentation and the implantation profile as indentation depth increases.

characteristics were done by hand using the Digital Micrograph software to measure size correctly and Leica Application Suite with LAS phase expert module and Image Analysis module to obtain the distribution density.

3. Results

3.1. Nanoindentation

Nanoindentation matrices were performed on each disc at a given irradiation temperature at a maximum penetration depth of 500 nm in at least three areas of the implanted surface with a separation between indentations larger than three times their edge, avoiding plastification volume overlapping. To analyze the hardness variation with good accuracy the very first nanometers were not taken into account because the curves presented some intrinsic phenomena to the technique itself that causes a high scatter in the results and consequently were not representative. In a previous work conducted on the materials studied in this work, it was concluded that both EUROFER97 and EU-ODS EUROFER presented indentation size effect (ISE) on the as-received state [19,34] which explained why these materials showed a change in nanoindentation hardness values with depth as shown hereunder. The results obtained with all the nanoindentation tests were processed using Analyst software provided by MTS [27] with which error and average values were calculated.

3.1.1. EUROFER97

In Fig. 6a, hardness values vs indentation depth after He

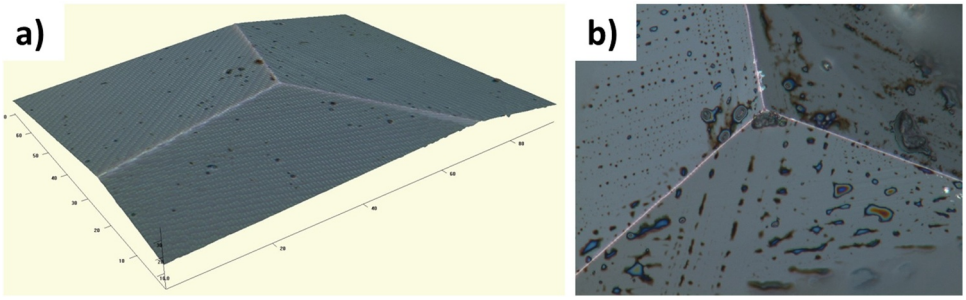

Fig. 3. (a) Berkovich indenter tip profile obtained by a confocal microscope, (b) detail of the very tip.

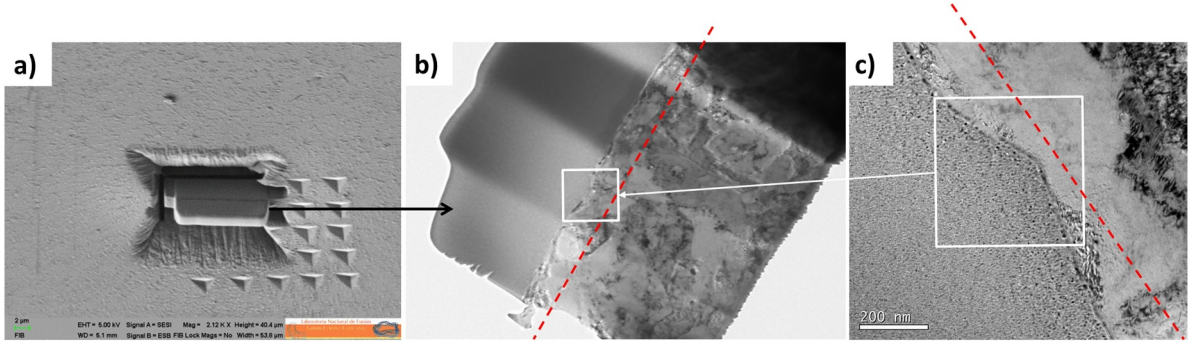

Fig. 5. FIB lamella extraction by the lift-out procedure from a nanoindentation matrix (a) analyzed by TEM (b). Detail area of the cross-section of nanoindentation (c). Implantation depth is highlighted with a red dashed line.

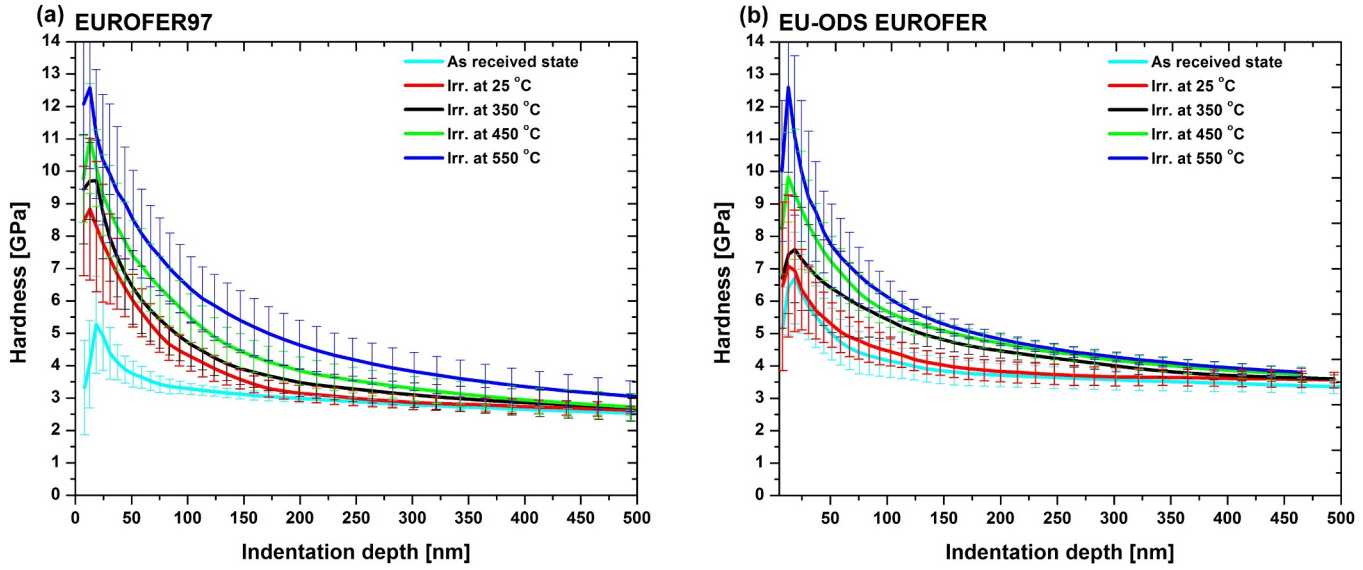

Fig. 6. EUROFER97 (a) and EU-ODS EUROFER (b) hardness values vs indentation depth of the as-received state, and after implantation with He at RT, 350 °C, 450 °C and 550 °C.

implantation at different irradiation temperatures (RT, 350 °C, 450 °C and 550 °C) are plotted, including the results of the as-received state. All the specimens showed a hardness increase after irradiation below ~400 nm (in contrast, for the whole tested depth for the sample irradiated at 550 °C), the higher the irradiation temperature, the higher the increase.

In the as-received state (unimplanted condition) the maximum hardness value measured was 5.3 ± 1.5 GPa, and after He implantation the maximum hardness values measured were as hereunder: 8.9 ± 2.2 GPa (RT), 9.7 ± 1.2 GPa (350 °C), 11.0 ± 1.7 GPa (450 °C) and finally 12.6 ± 2.5 GPa (550 °C). All of these results were obtained at a depth around 30 nm to 50 nm. At 150 nm, which is the depth where He concentration is maximum (~800 appm He according to MARLOWE simulation), the nanoindentation hardness measurements were 3.1 ± 0.1 GPa, 3.6 ± 0.3 GPa, 3.9 ± 0.5 GPa, 4.5 ± 0.5 GPa and 5.4 ± 0.9 GPa corresponding with the as-received status, and implanted at room temperature, 350 °C, 450 °C and 550 °C, respectively.

3.1.2. EU-ODS EUROFER

Results for EU-ODS EUROFER are given in Fig. 6b for all the irradiation temperatures (analogously to EUROFER97). Analyzing the curves, in the as-received state, a maximum hardness value of 6.7 ± 1.5 GPa was obtained. After He implantation, the maximum hardness values measured for all the conditions, were 7.1 ± 2.2 GPa (RT), 7.6 ± 1.6 GPa (350 °C) and 9.8 ± 1.4 GPa (450 °C) and 12.6 ± 2.6 GPa (550 °C) approximately at the same depth than EUROFER97. Making the same analysis at 150 nm (maximum He according to simulations), hardness values were 3.8 ± 0.4 GPa, 4.0 ± 0.3 GPa, 4.8 ± 0.3, 5.1 ± 0.3 GPa and 5.3 ± 0.3 GPa corresponding with the as-received status, and implanted at room temperature, 350 °C, 450 °C and 550 °C respectively.

It may be deducted from the aforementioned graph that the highest hardness value is measured at 550 °C. However, the difference between the hardness at RT (red curve) and at 550 °C (dark blue curve) is smaller than the one observed in EUROFER97. In addition, beyond 350–400 nm, the nanoindentation results are almost the same as in the as-received state (light blue curve). EU-ODS EUROFER steel shows a softer trend of hardness values curves to reach the hardness values on the as-received state than EUROFER97, which is more pronounced. Regardless of the irradiation temperature, in all the experiments of both materials, the as-received hardness value is reached at the same depth (around 500 nm) which validates the limit depth chosen for the nanoindentation tests.

3.2. Microstructural characterization

3.2.1. TEM characterization of EUROFER97

The detection of cavities in the He implanted EUROFER97 at RT (Fig. 7a) was complicated regardless of the distance from the surface (and hence, the He concentration) due to their small size (1.7 ± 0.3 nm). A high error must be considered for cavity sizes below 1 nm due to the amount of defocus used to detect them [35] that

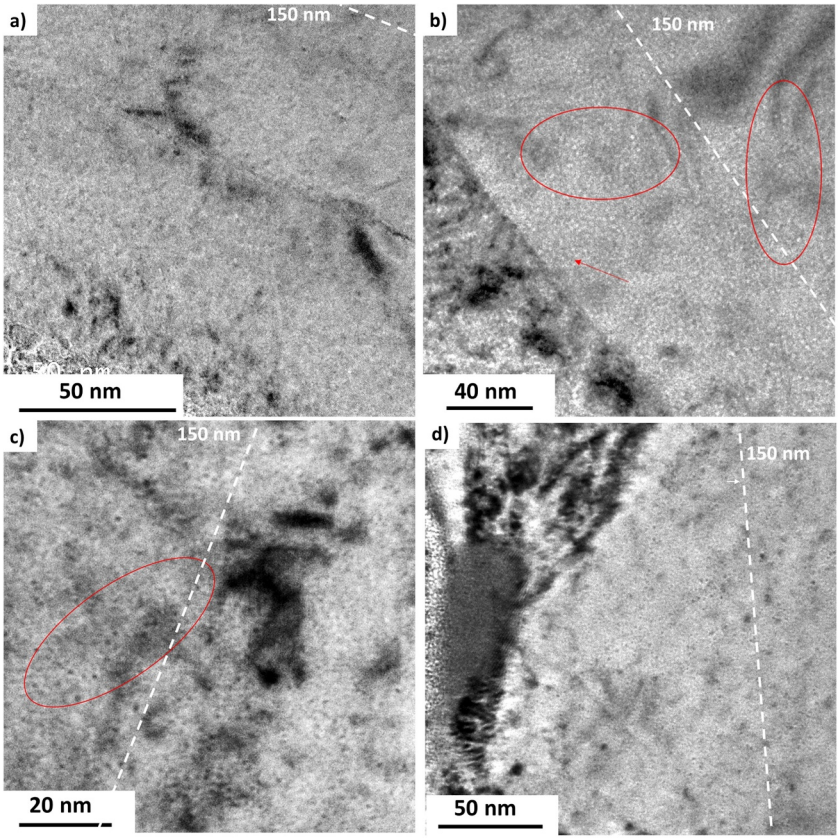

Fig. 7. TEM images showing characteristic cavities of EUROFER97 implanted with He at 40 kV at (a) RT, (b) 350 ˚C, (c) 450 ˚C, (d) 550 ˚C. Images taken in underfocused (a-b) and overfocused (c-d) condition. Red circle in Figure 7 b, represents some allignment or cavity clustering, and in Fig. 7c a clear allignment. In both cases nearby the implantation peak.

depending on the specimen thickness its value was between 500 nm up to 1 μm in absolute values. To calculate size and distribution density all the cavities detected from the surface up to the 300 nm depth were counted since there have been no more cavities detected beyond. In addition, that depth was in a good agreement with the Marlowe profile simulation. Their population density increases almost proportionally with the amount of implanted He showing a peak between 150 nm and 200 nm as the simulated profile predicted. The population density in the whole irradiated area of was 1.09×10^{22} m^{-3}. Random distribution was found, they seem not to be attached to any microstructural sinks which would indicate that the nucleation was preferential.

At 350 ˚C more cavities were observed randomly distributed within the matrix as well as an increase of small groups were detected in comparison with the observations made in EUROFER97 implanted with He at RT (Fig. 7b). There is a slight increase in terms of size, 2.1 ± 0.4 nm and population density, 1.96×10^{22} m^{-3}. The observations performed by TEM did not reveal preferential nucleation on grain/subgrain boundaries and/or precipitate-matrix interface. Although a tendency for preferential nucleation has not been observed, the possible association of some cavities (or embryos) to sinks cannot be ruled out.

Microstructural observations of EUROFER97 steel implanted with He at 450 ˚C indicated a turnaround in terms of the distribution of the cavities and even in the cavity population density along with an increase up to 5.86×10^{22} m^{-3}. With respect to the distribution, cavities could be identified from the very beginning of the lamella until near the end of implantation volume, ~300 nm in depth. In addition, an alignment is detected which would indicate preferential nucleation; however some randomly nucleated cavities were also detected, as observed in (Fig. 7c). However, it was not possible to assert if the alignment was due to dislocations in the material which act as a defect sinks or to another microstructural features. These results showed that under these experimental conditions two types of cavity nucleation may exist simultaneously: isolated and aligned nucleation respectively, even though the bubbles size was the same order to the previous experiments at lower irradiation temperature, which was calculated as 1.9 ± 0.4 nm. Detecting aligned cavities is an indication that under these experimental conditions of irradiation at 450 ˚C, the effect of any defect sinks seems to be enhanced by the irradiation temperature, since temperature promotes diffusion. Interfaces, grain boundary precipitates and/or subgrains within the implanted area were analyzed exhaustively. An example of this behavior of preferential nucleation on a MX is shown in Fig. 8, where several cavities highlighted with a red oval were observed in the MX/matrix interface.

Finally, at 550 ˚C the microstructure showed cavities with similar mean size than the observed ones at 450 ˚C, which was 2.3 ± 0.7 nm. However, in this particular case, larger cavities up to 4 nm have been detected as well, which would indicate the cavities have experienced a

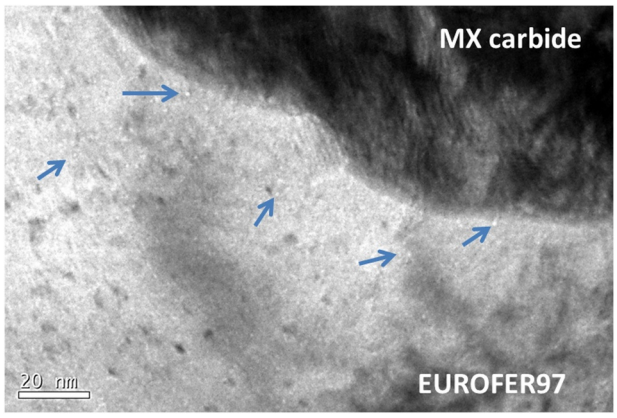

Fig. 8. Microstructure of EUROFER97 implanted with He at 40 keV at 450 ˚C showing a MX-type carbide interface with both cavities attached to it and also nucleated within the matrix.

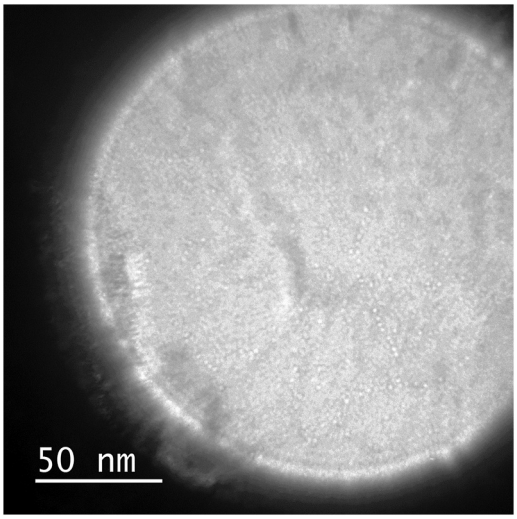

Fig. 9. Microstructure of EUROFER97 implanted with He at 40 keV at 550 °C showing the alignment of cavities within the matrix, obtained with ARM JEOL 300 kV.

slight growth as a consequence of irradiation temperature. The microstructural observations showed cavities with a much more pronounced alignment, Fig. 9, possibly along dislocations or sub grain boundaries which were not observed because of the microscope conditions, since to reveal dislocations depending on their nature it is necessary to tilt the sample in order to fulfill certain crystallographic conditions [36,37]. Regarding population density the majority of cavities have been detected within the ion range depth, although from 200 nm in depth they were clearly more difficult to observe. In addition, some cavities nucleated near the irradiated surface, approximately between 50 and 60 nm where the displacement damage and the He concentration were low. In this case the population density was 4.029×10^{22} m^{-3}, which seems to indicate that there is a maximum in terms of nucleation at 450 °C and at 550 °C cavities started to grow slightly.

3.2.2. TEM characterization of EU-ODS EUROFER

EU-ODS EUROFER steel implanted with He at RT exhibits a random distribution of cavities within the area of highest He concentration (600–800 appm) located approximately between 100 and 200 nm from the implanted surface. In some other areas clusters of cavities were observed, while in others the cavities were isolated. It is possible to observe in Fig. 10a) along with two clusters of cavities, marked with red ovals, the zone with a highest He amount (~800 appm He). The size of cavities detected was very small, 1.8 ± 0.3 nm. Regarding population density, most of the cavities were found between 100 and 200 nm depth which matches with the implantation peak placed mentioned above, although, nearby the surface of implantation some cavities were detected as well. Nevertheless, the value of the cavity population for the whole implanted volume was 1.63×10^{22} m^{-3}. Regarding cavity formation at grain boundaries, nucleation at these microstructural features was also completely random. Fig. 11 shows a TEM micrograph where Yttria ability of acting as a defect sinks throughout the whole irradiation volume is described perfectly on EU-ODS EUROFER irradiated at RT. Cavities attached to the interface of some oxides were observed, however, in the implanted area other Yttria particles but free of cavities in their respective interfaces were also detected. It seems that the behavior of these oxides, in terms of trapping cavities, irradiation conditions are purely random, at least under these experimental conditions.

Microstructural observations of the lamella extracted from the EU-ODS EUROFER steel implanted with He at 350 °C showed the same population density of cavities as the one irradiated at RT,1.87×10^{22} m^{-3}. However, there seems to be a slight increase at the implantation depth where the concentration of He is maximum. Fig. 10 shows representative micrographs of the cavities detected within the implanted volume of material. The cavities are small with an average size of 1.9 ± 0.5 nm which means that there is no noticeable change in comparison with the irradiation at RT. However, notable increase of population density between 100 nm and 250 nm in depth with respect to other areas with lower He concentration where cavities were also detected but the population density was much smaller is noticed in a qualitative way. On average, in all the irradiation depth, the density is in the same order of magnitude as in the RT experiment. With respect to the nucleation of cavities in microstructural features that act as sinks, a clear trend was not observed which would indicate a special difference with the implantation at RT. Isolated cavities have been detected nucleated at grain boundaries, similar to the ones observed in yttrium oxides.

The microscopic observations at 450 °C revealed a microstructure completely different compared to all the ones studied so far in this research. From the surface of the sample, many cavities were detected with a random distribution and a much higher density than in the previous cases already analyzed (implantation at RT and at 350 °C respectively) where most of the cavities were located, especially in the area of the largest concentration of He. In fact, the population density increases more than one order of magnitude up to 4.87×10^{23} m^{-32}. In addition, it was detected the existence of large amounts of near-surface cavities, along with some cavities observed near what should be the implantation limit depth, which is around 300 nm.

The average size is 2.4 ± 0.6 nm, although in some cases (the rarest ones) the cavities seem to have a larger diameter of up to 4 nm. In most of these cases at this irradiation temperature, the EU-ODS EUROFER microstructure is decorated with cavities aligned along some kind of microstructural feature, such as dislocations, producing a “string of pearls”. This observation is reflected in the red ovals drawn in Fig. 10a–c.

Under these experimental conditions, cavities nucleated at grain boundaries and interfaces including yttrium oxides were clearly detected. However, due to the large increase in population one cannot state whether the cavities nucleated in those places attracted by the mentioned sinks or by chance since population increased remarkably. Regarding yttrium oxides, no particular trend about acting such as sink defects was detected, since the surrounding area of the Y_2O_3-matrix interface is not depleted of cavities. Consequently, it is not possible to conclude that during the irradiation under these particular conditions, Yttria particles acted as sinks.

Finally, EU-ODS EUROFER at 550 °C showed another turnaround regarding size and distribution of cavities. After an exhaustive analysis of the microstructure, it can be said that the cavities were distributed both as clusters of cavities with different diameters (the most) and as isolated cavities within the whole volume of implementation, but in a completely random manner. The mean cavity size is 4.9 ± 1.5 nm, with some detected cavities of up to 7 nm, and their population density was 1.15×10^{21} m^{-}. These results indicate that the growth is much more enhanced than the nucleation under these experimental conditions.

All the grain boundaries contained in the implanted area within the lamella were studied, as the one that is shown in Fig. 10c completely crossing the whole implanted area. Throughout it, one can observe that the boundary has attached some cavities as observed in the same figure highlighted with red arrows. However it is possible to notice that other cavities have nucleated very close which seems to suggest that the nucleation process was random, since the depletion area along the grain boundary was not clearly identified.

Some large cavities were highlighted with a red box in Fig. 10d. They were found at approximately 300 nm of depth from the surface. Compared with the implantation profile, that depth would be the maximum implanted depth. Fig. 12 shows in detail this part of the implanted area, by means of a through-focus series at higher magnification. The cavities were not detected in on-focus condition, which represents a first indication of the maximum diameter, less than 5 nm,

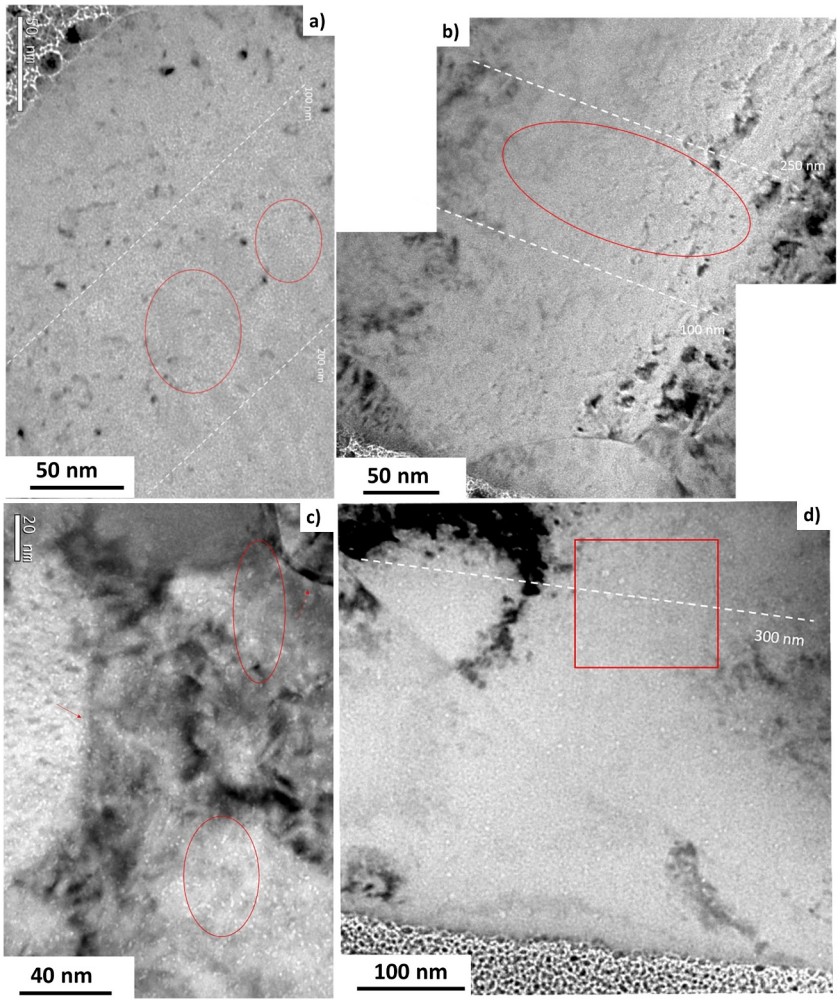

Fig. 10. TEM images showing characteristic cavities of EU-ODS EUROFER implanted with He at 40 kV at (a) RT, (b) 350 °C, (c) 450 °C, (d) 550 °C. Images taken in underfocused condition (defocus between 0.5 μm and 1 μm). Large cavity clusters are highlighted with red figures. There are some cavity clusters highllighted with red ovals in a, b and c. On the other hand, red arrows in c pointed to some cavities alligned in boundaries. Finally, the red square in d showed as at 550 °C, there are some large cavities just at the end of the implantation zone, 300 nm.

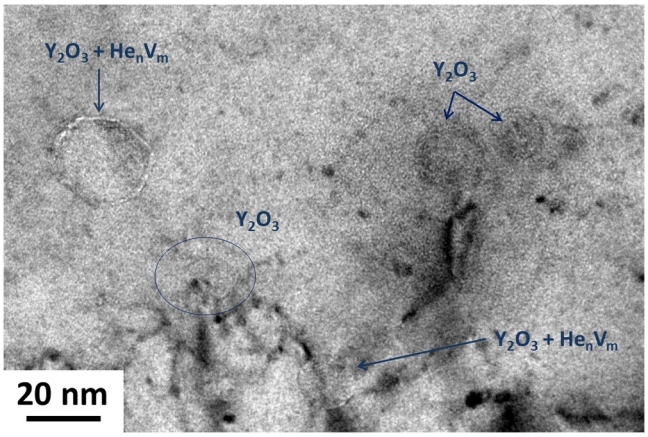

Fig. 11. TEM micrograph of EU-ODS EUROFER implanted with He at 40 keV implanted at RT showing yttrium oxides taken under focused (500 nm) in bright field condition with and without cavities on their boundaries.

even although measuring directly onto the micrograph the diameter is larger. Due to their diameter, however, it is possible to think that those microstructural features are oxides instead of cavities, but after performing through-focus series, that possibility was removed. Furthermore, it is worth noting the detection of cavities very close to the surface which were between 3 and 4 nm in size.

To summarize, Table 1 presents all the studied features for all the cavities clearly detected within the irradiation depth (~300 nm) such as: average size and standard deviation, distribution density and how the cavities are distributed for EUROFER97 and EU-ODS EUROFER irradiated at 40 keV and RT, 350 °C, 450 °C and 550 °C.

4. Discussion

The nucleation and growth of cavities filled with helium atoms, as well as their influence on the deterioration of the mechanical properties of structural materials for fusion applications has been studied thoroughly using different irradiation methods such as ion implantation, fission neutrons [38,39] or spallation sources [40]. It has been observed that bubbles nucleate even at low concentrations of He (with concentration around 10 appm) and at very low damage values, $\sim 10^{-3}$ dpa, the final microstructure being strongly dependent on the implantation temperature [41], as observed in this research. There is evidence that these cavities grow as both the concentration of He and the damage rate increases while maintaining an almost constant population density after passing the peak of the initial nucleation. Bubbles absorb He atoms from the matrix solution increasing its density and size rather than allowing the creation of new bubbles (self-limitation) [17,42]. At higher He concentrations, this effect is negligible compared

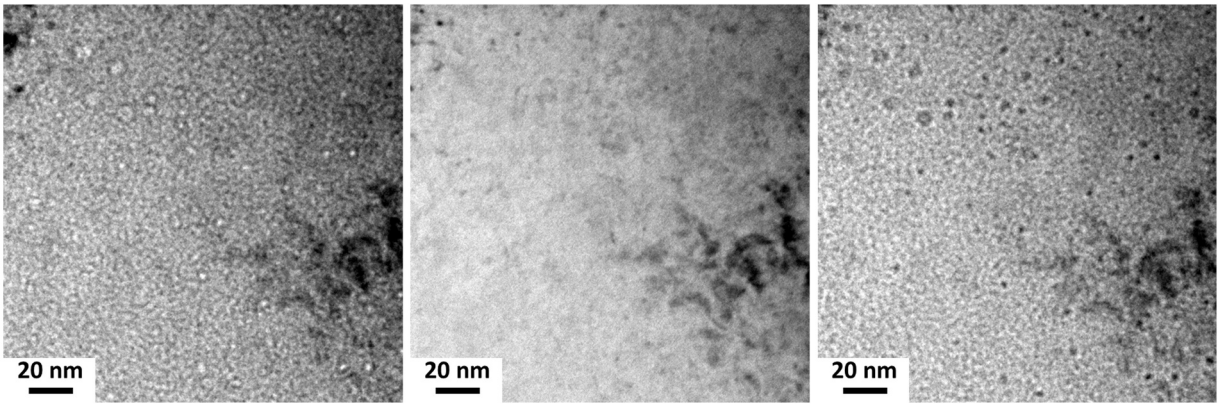

Fig. 12. TEM though focus series micrographs of the red square from Fig. 10, which was taken from EU-ODS EUROFER implanted with He at 40 keV and 550 °C. (a) Underfocused image −200 nm (white cavities) (b) on focus image (no cavities revealed) (c) overfocused image +200 nm (black cavities). No Ytria observed.

Table 1
Summary table of cavity features for EUROFER97 and EU-ODS EUROFER irradiated with He at 40 keV and different temperatures.

Material		RT	350 °C	450 °C	550 °C
EUROFER97	Average size [nm]	1.7 ± 0.3	2.1 ± 0.4	1.9 ± 0.4	2.3 ± 0.7
	Population density [10^{22} m^{-3}]	1.09	1.96	5.86	4.029
	Distribution	Random	Random + small clusters	Random + Aligned	Aligned
EU-ODS EUROFER	Average size [nm]	1.8 ± 0.3	1.9 ± 0.5	2.4 ± 0.6	4.9 ± 1.5
	Population density [$10^{22}m^{-3}$]	1.63	1.87	48.7	0.15
	Distribution	Random	Random	Random. Increase in nucleation	Random. Increase in size

to the number of new bubbles generated by the implantation (vacancy generation), since the re-solution (in terms of dissociation) of He from the already nucleated bubbles will cause the nucleation of the second generation of bubbles. For metals implanted with He at intermediate irradiation temperatures between 0.2 and 0.5 of the Fe melting temperature, there is convincing evidence about this phenomenon in existing bubbles due to displacement cascades [13]. Indeed, experiments seem to indicate that an increase of dpa values implies an increase of population density of bubbles produced by the re-solution and nucleation of new cavities [13].

In the experiments carried out in this research the atomic damage was low, $\sim 10^{-1}$ dpa. In addition, the damage rate and the final He concentration were kept as constant as possible with the goal to evaluate the evolving cavity distribution and size only as a function of irradiation temperature. According to Trinkaus et al. [41] for low He/dpa rate, the population density of bubbles does not seem to depend significantly on the concentration of He or the irradiation time while the average bubble size increases continuously when the defects are visible by means of TEM. This fact indicates that nucleation occurred and then suddenly stopped, favoring growth. It was suggested as well that the characteristic parameters of the bubble growth vary during implantation experiments. The nucleation process is determined by the phenomenon described previously as self-limiting. After a peak nucleation, both the nucleation rate and the concentration of He in the solution in the matrix decreases, being more drastic at first. While the density appears to be reaching a stable value and the average radius is continually growing.

In general terms, EUROFER97 and EU-ODS EUROFER implanted at 40 keV presented a trend in population density similar to the implantation profile, which means that the population density increases with depth, as Fig. 2 predicted. Taking into consideration the research conducted by Yang et al. [43] did observe the implantation profile coincided roughly with the TEM observations, detecting an area with a maximum concentration of cavities. Furthermore it is noted that for a shallow implantation of the order of keV, the radiation damage occurs near to the very surface, which explains the detection of cavities within the first nanometers of the implanted surface. More specifically when comparing a bulk irradiation with a very shallow one, the type of irradiation defects produced and even the morphology of the damage peak is different [44,45], because the defects are attracted to the surface which explains more accurately why cavities are found close to the irradiation surface. Finally, another remarkable observation was the different distribution of cavities produced at 450 °C and 550 °C depending mostly on the material microstructure. Edmondson et al. [46] performed another He implantation on a new ODS that belonged to nanostructured ferritic alloys (NFA) family. However, the amount of He introduced is by far much larger than in the present research, reaching at its maximum of 12 at.%. But, in regard to the implantation profile, a similar conclusion is obtained, the population density increases as depth does.

One of the most important parameters when characterizing radiation resistance structure is the metal matrix phase, since one material may exhibit inherently more resistance to accumulate radiation defects [47] depending on this. In the case of steel, face centered cubic crystal structures (FCC) would contain higher defect concentration than body centered cubic structure (BCC) and hexagonal close packed structure (HCP) but due to irradiation anisotropic growth issues are excluded for nuclear applications [48,49]. In fact, one of the main reasons to discard FCC steels as Nuclear Fusion structural materials is their much lower swelling resistance than BCC steels [50]. Both EUROFER97 and EU-ODS EUROFER present BCC structure, however, the martensitic structure is a distorted BCC which is denoted as BCT. Nevertheless, this distortion seems to be less critical to irradiation defect gliding and storage than the fact of presenting many more vacancies within the matrix, as observed on EU-ODS EUROFER.

Under the irradiation conditions on this research, EUROFER97 steel showed cavities on its martensitic microstructure aligned in what appear to be dislocations (as seen in Fig. 9 since no subgrain boundaries were observed, so only dislocations may fix the cavities); however the cavities in the EU-ODS EUROFER steel were grouped in clusters in a more random manner, since its complex microstructure has large number of possible traps for He, resulting in formation of tiny cavities in the matrix, avoiding the migration to grain boundaries [51]. This behavior is also observed by Ryazamov et al. [52] although in that

experiment the cavity nucleation and eventually growth effect is more exacerbated since the He ion energy is higher than 3 orders of magnitude (60 MeV) so the irradiation depth results much larger, so the probability of finding Yttria particles within the irradiation profile is much higher, and hence the possibility of studying their trapping effect is increased. Regarding the sink strength, in theory, the interface between matrix and oxide particles can act as efficient trapping sites for point defects and helium atoms. Increasing matrix-oxide interfaces the material may enhance the defect combination and disperse helium atoms, thus minimizing the well-known helium embrittlement and diminishing void swelling [50]. Nevertheless, under the irradiation conditions carried on in this research, it seems that the grain (or subgrain) boundaries are more efficient than oxide interfaces to trap cavities at all irradiation temperatures.

In an irradiation experiment with He at 100 keV up to 0.8 dpa at room temperature and at 350 °C conducted by Luo et al. [53], no cavities were observed within the material, which was a RAFM steel named SCRAM. Generally speaking it has similar microstructure but some differences in terms of composition in comparison with EUROFER97 (9.24 Cr, 2.29 W, 0.49 Mn, 0.25 V, 0.25 Si, 0.088 C and 0.0059 P; larger Cr and W, similar Mn, V, and no Ta). However, when the material was irradiated at temperatures at 450 °C, cavities nucleated and grew along microstructural sinks, such as dislocations, grain and/or sub-grain boundaries and precipitates. On the other hand, it is possible that the cavities were too small (embryo-like) and therefore their size was below the resolution limit of the conventional microscope which strongly depends on the sample. Fig. 13 shows a through-focus series micrograph taken from the EUROFER97 sample irradiated at 40 kV and 550 °C where some very small cavities are discovered, similar to the order of magnitude of the aforementioned embryos-like cavities. The accumulation of those cavities, extremely hard to observe by conventional TEM, added an extra component to the increase of hardness measured by nanoindentation, since they are dislocation barriers. This discovery makes the good agreement between microstructural observations and mechanical results more consistent. In any case, microstructural observations of specimens irradiated at high temperature are consistent with those ones shown in this research. With increasing irradiation temperature an arrangement of cavities along nucleation sites in the case of EUROFER97 was favored. In the case of EU-ODS EUROFER at 450 °C very high nucleation throughout the matrix happened, possibly because the high concentration of traps (dislocations and vacancies own of the material itself due to its fabrication route). At 550 °C which appears to occur is a growth of cavities instead of the nucleation of new ones, again protecting grain boundaries, so an eventually structural damage may be diminished. In the future Nuclear Fusion Reactors, helium cavities shall be formed under stresses; and it is well known that these cavities tend to preferentially form at grain boundaries where they can cause pronounced loss of strength because of a grain boundary decohesion. This undesirable effect is known as high temperature helium embrittlement (Ullmaier 1984), and it might be diminished if He cavities nucleated in the metal matrix and remained immobile. For tensile strain rates near 10^{-4} s^{-1} and test temperatures near 550 °C, helium embrittlement of grain boundaries is induced for helium concentrations near 100 appm in austenitic stainless steel whereas grain boundary embrittlement is not observed even with 1000 appm He in ferritic/martensitic steel (Yamamoto et al. 2002).A similar observation is achieved by Edmondson et al. [46] where they found bubbles nucleated at dislocations (~12%) and grain boundaries, but in a smaller amount than the ones nucleated within the matrix, as reported here.

In the irradiation experiments with an irradiation temperature of 450 °C and 550 °C, the ion current was higher than in the other two implantations (RT and 350 °C), which implied an increase in dose rate term. It is probably because of this increase, that in the case of implantation at 550 °C is almost doubled (as mentioned in the irradiation description) compared with the ones implanted at room temperature and 350 °C respectively, variations in the generation and fate of microstructural defects may occur. This parameter has been studied in numerous publications with different materials such as austenitic steels irradiated with neutrons [54,55] or model alloys irradiated with heavy ions [56] among others. However, despite these studies a clear correlation between microstructural modification and damage rate variations has not been demonstrated. It seems that for a given temperature and He concentration, experimental data indicates that the density of bubbles increases as size decreases when the production rate of He is increased [41]. Considering the microstructural observations it is difficult to discern how the increase of implantation rate of He has affected to the cavities evolution, since for a study of this variable the temperature should have been kept fixed and only the damage rate should have been modified, since the value of the temperature may enhance the generation of cavities/bubbles or conversely may inhibit if the temperature is too high [41,57].

Regarding irradiation temperature, it has been demonstrated that it is a very important parameter in the nucleation and evolution of cavities [41]. The results of the TEM investigations performed for this paper showed with an increasing irradiation temperature an increase in the cavity population. However, EU-ODS EUROFER steel implanted at 450 °C showed an increase of bubble density respective to the experiments at RT and 350 °C, possibly caused by the large number of vacancies inherent to its microstructure [58] which increased their

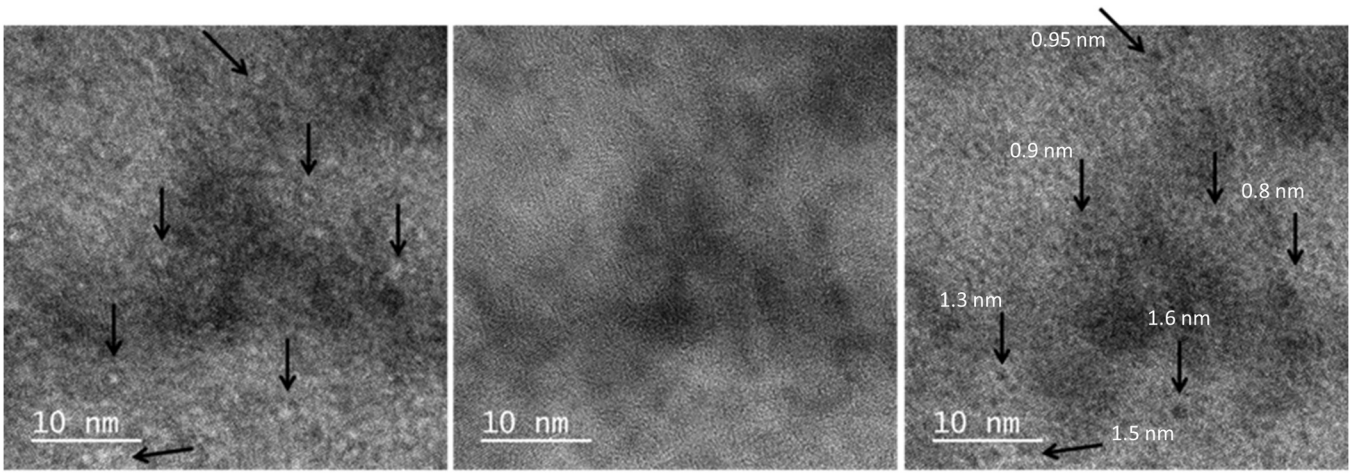

Fig. 13. Atomic resolution micrograph obtained with JEOL ARM 300 kV of EUROFER97 irradiated at 40 kV and 550 °C pointing with arrows some very small cavities with a size ≤ 1 nm (underfocused, on focus and overfocused, ± 400 nm).

mobility by diffusion with increasing temperature. This agrees with the fact that the implantation of EUROFER97 is maintained within 300 nm showing a gradient in the cavity density which seems to be proportional to the concentration of He (even at the highest temperature), whereas in EU-ODS EUROFER the entire implanted volume (300 nm) is equally filled with bubbles. These observations indicate a behavior drastically different in terms of nucleation cavities at high temperatures in both materials. However, EU-ODS EUROFER experienced a remarkable cavity size growth at 550 °C which matches with the population decreasing.

From an engineering point of view, it is necessary to correlate the microstructural observations in terms of the evolution of the cavities produced by the implantation with the changes detected in the material hardness. Although extrapolation of nanoindentation results to macroscopic properties such as yield strength or strain hardening coefficient is not straightforward [59,60], nanoindentation is a powerful tool which permits quantify the effect of the irradiation temperature on the mechanical response of the material.

It was published elsewhere [6] that both materials presented in the as received state an effect called indentation size effect (ISE) which is due to its inherent characteristics of ductility, strain hardening, etc. In nanoindentation, this effect is characterized by a decrease in hardness values with depth of penetration, being more significant in the first nanometers up to reach a value in which these values are stabilized. This effect has to be taken into account very carefully when indenting materials irradiated very shallowly.

In order to quantify the effect of implantation of He at different temperatures in steel EUROFER97 and EU-ODS EUROFER, it was defined the ratio H_{IRR} / H_{UNIRR} dividing the values of average hardness obtained for each irradiation at each temperature between material hardness values of the as received state in function of penetration depth. These results are depicted in Fig. 16a) for EUROFER97 and b) for EU-ODS EUROFER. Additionally, dotted lines indicating approximately the point of the highest hardness value for all the irradiation experiments have been drawn in the mentioned figures. This means that from that point the hardness decreases with penetration depth up to reach equilibrium depth, where the hardness values of the irradiated material matches with the as received state. In the case of irradiated EUROFER97, it has that peak approximately at 45 nm and EU-ODS EUROFER approximately at 65 nm far from surface.

Before correlating the microstructural changes produced by He implantation with nanoindentation values, it is important to gain insight about the relationship between indentation depth (the actual depth measured by the device through the piezoelectric system) and the volume affected by the indentation. Using different TEM/STEM contrasts, it was possible to perform a study about the distribution and depth of the dislocations produced by the imprint but only in a semi-quantitative way. It was not possible to make a proper quantification of the dislocation density due to the enormous quantity of dislocations found, likewise as reported elsewhere [61,62]. To distinguish between the dislocations produced by the indentation and the ones inherent to the material was unfeasible, however following the indentation direction, it was detected a certain area surrounding the indentation which contained most dislocations. Fig. 14 shows the microstructure just beneath of the indentation, where it is possible to observe some grains deformed along the indentation direction, Fig. 14a). In image Fig. 14b) the material defects are revealed as dislocation networks revealed in dark field. For an indentation depth of 120 nm it was observed a very high density of dislocations around the imprint up to a depth of 350–450 nm far from the vertex, as shown in Fig. 14b. So, on the basis of the results obtained it was assumed that most dislocations produced by the indentation would be found within an area whose radius would be between 3 and 4 times the indentation depth. Those observations were performed in both steels, EUROFER97 and EU-ODS EUROFER, taking into consideration that the crystals have to be tilted far from the Bragg condition, so the orientation contrast did not hide the dislocations.

In Fig. 15 shows another example, by using a STEM micrograph enhancing the dislocation contrast of another lamella extracted and thinned, including a detail of a nanoindentation cross section, which formed part of one of the matrix performed on EU-ODS EUROFER. In the mentioned figure it is possible to observe the maximum depth of the implantation area, highlighted with a red dotted line, and the high dislocation density contained in a red circle which is far from the indentation approximately 4 times the indentation depth. In these materials it is hard to quantify perfectly because of the high density of dislocation barriers as grain boundaries, other dislocations, etc. But in order to compare the nanoindentation results, those observations corroborate the hypothesis.

Given the irradiation profile, Fig. 2, the depth with the highest He content is placed at approximately to 150 nm from the surface, which a priori, coincides with the estimation that the volume of plasticization is about 3 to 4 times the indentation depth, as indicated in Figs. 14 and 15.

Comparing these results by nanoindentation with the microstructural TEM observations, it is observed that EU-ODS EUROFER has cavities beyond implantation depth of the profile calculated by MARLOWE when the irradiation temperature was 450 °C, Fig. 10c), and 550 °C, Fig. 10d) respectively. However, in EUROFER97 the cavities were not detected so clearly. It seems that due to the high irradiation temperature the volume with the highest cavities concentration on EU-ODS EUROFER has been moved deeper compared to EUROFER97, this was cause by a diffusion process boosted by the microstructure, similar to the transition line measured by nanoindentation.

Moreover, as already mentioned, it should be noted that in the first nanometers some artifacts that invalidate the measurements may appear and therefore must be discarded or at least minimized, such as a slight but hard oxidation layer (although in this case the irradiation was carried out in high vacuum and no discoloration was observed on the surface of the sample), sample roughness etc. It has been determined that valid results started from approximately 10 to 15 nm depth.

For samples implanted very superficially and indented afterwards on a normal surface to the ion beam, the H_{IRR} value is a key parameter, because it indicates to what depth the volume affected by the indentation (plastic deformation) reaches, as seen in the schematic representation of Fig. 4. It should be emphasized that the assumption of a hemispheric volume containing all the plastic deformation is not a very accurate approximation. It has been observed in several studies carried out with different metals and subsequent analysis with EBSD that depending on the crystallographic orientations and even on the microstructure, the dislocations flow varies and therefore also its distribution [63–65]. Even so, a correlation between the maximum hardness value obtained by nanoindentation and the microstructural observations was done taking into account the aforementioned assumption. Regarding Fig. 16, for the He implantation at 40 keV the transition line was located approximately between 40–50 nm for EUROFER97, and 60–70 nm in the case of EU-ODS EUROFER, which turns out at about 1/3 to 1/4 of the maximum He concentration depth. These results are in a very good agreement with observations made by TEM of the indentation cross sections.

The material microstructure is a fundamental aspect to consider when one wants to perform these types of correlations. In similar studies, such as in Fe Cr alloys with low dislocation density [66], it was detected that the radius of the plastic volume was located at 10 times the indentation depth without implantation. On the other hand, after Fe implantation to produce irradiation damage, the radius of the plastic volume was between 3 and 4 times. So, there is a clear effect between dislocations interacting. However, unlike the results presented in the aforementioned research, Tanigawa et al. [67] did not manage to make the same estimation of the volume affected by the indentation and

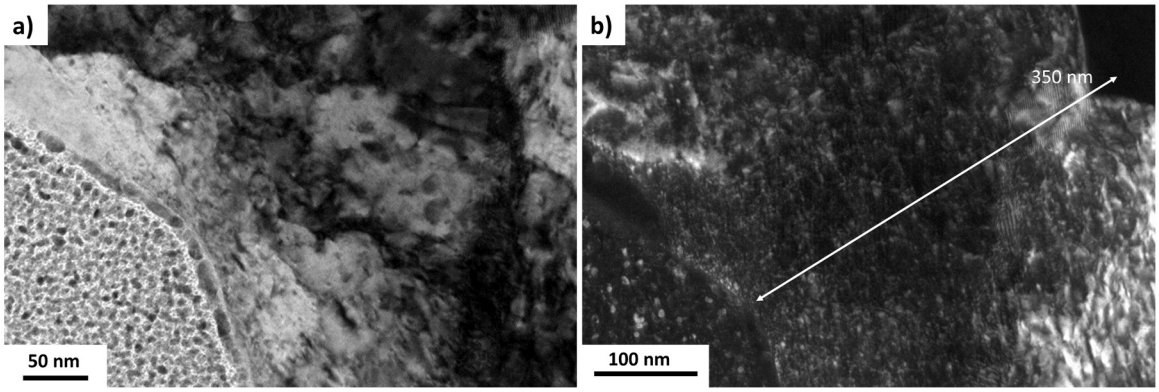

Fig. 14. TEM micrograph of a transversal section of a nanoindentation of EU-ODS EUROFER implanted with He using (a) bright field and (b) dark field.

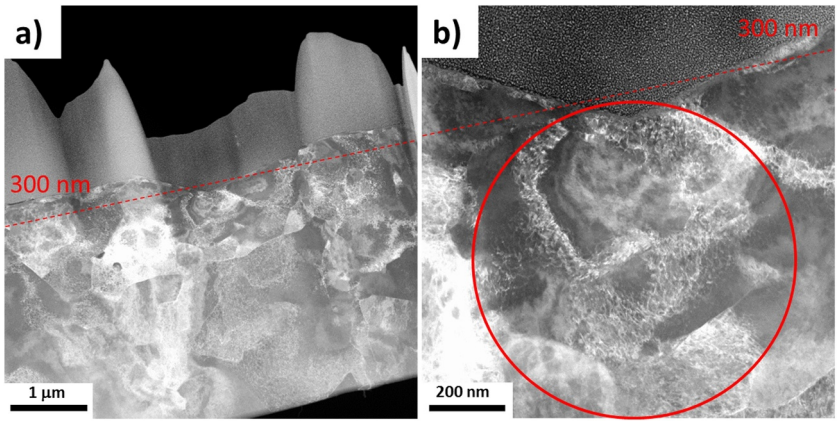

Fig. 15. ADF-STEM micrograph of a lamella extracted by means of FIB from a specimen irradiated with He including the transversal section of a nanoindentation, (a) detail of the lamella and (b) close up of the dislocations under the indentation.

penetration depth for a F82H irradiated with Fe, which is much more similar to the materials studied here. This is because the natural dislocations (due to its own nature) presented into the material play an important role in the accommodation of the dislocations produced by the indentation as seen in these results.

Obviating the very first nanometers from nanoindentation tests, where some artifacts usually take place, as the indenter penetrates using the continuous stiffness method, causes that the plastification volume radius around the imprint, assuming a hemispherical volume, h_{IRR}, also increases, interacting with the damaged microstructure due to implantation up to reach certain depth where the hardness increase is maximum. The hardness values obtained will experience an increase, represented by an increase of the H_{IRR} / H_{UNIRR} ratio. This phenomenon is known as damage gradient effect (DGE). It happens because the microstructural damage caused by implantation with ions is not homogeneous and it presents a maximum at a certain depth from the

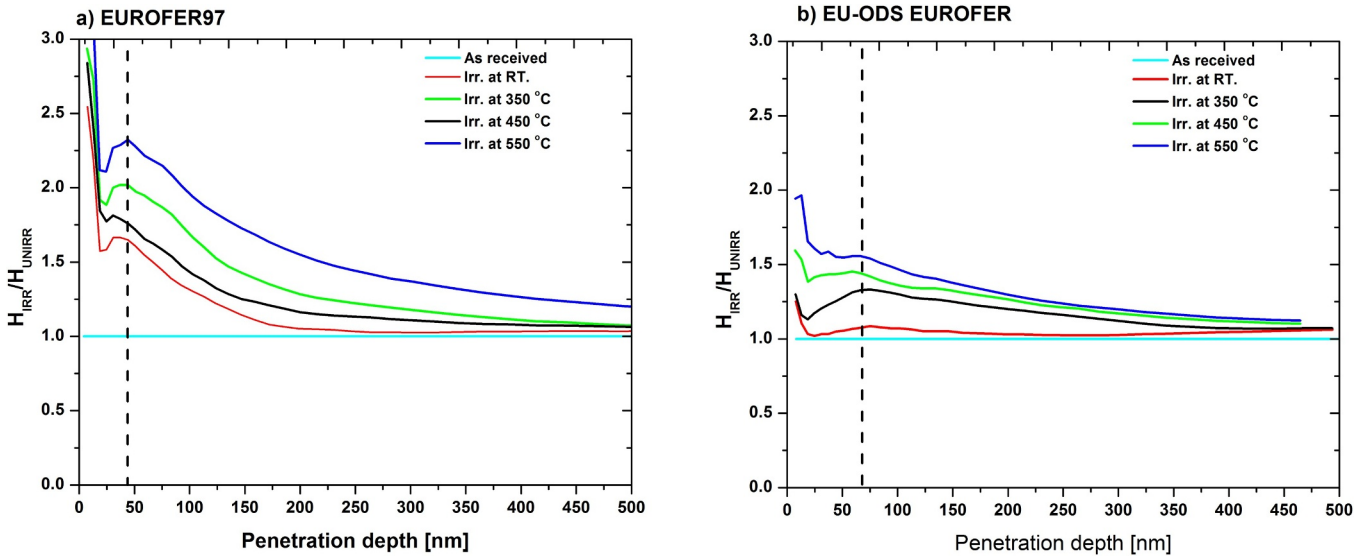

Fig. 16. Depth dependence of H_{IRR}/H_{UNIRR} ratio in (a) EUROFER97 and (b) EU-ODS EUROFER irradiated with He at room temperature, 350 °C, 450 °C and 550 °C.

surface which will depend on the ion energy. On the other hand, the damage profile will be dependent on ion mass, being completely different to one implantation of He at 40 keV with respect of another one of Fe at the same energy. At the moment h_{IRR} is deeper than the transition depth, Fig. 4, then, an overlapping will begin to occur between the defects of the most damaged volume produced by irradiation, and therefore the material will be more resistant to penetration, and the volume underneath with less damage until the unirradiated material is reached, making the ratio H_{IRR}/H_{UNIRR} decreases. This behavior is defined as softer substrate effect (SSE) studied extensively by other authors [68–70] which fits completely with the results obtained for EUROFER97 and EU-ODS EUROFER implanted with He.

Another important issue to consider when shallow implantations are performed, and afterwards when the mechanical properties are studied by nanoindentation on the normal surface to irradiation; it is the possibility of analyzing how to vary the indentation size effect due to irradiation. This is feasible (but tough to interpret completely) since the whole volume irradiated is located within the indentation volume. To explain the aforementioned phenomena in homogeneous materials, a model was proposed. This theoretical model is known as a Nix and Gao model [71]. It is based on the concept of geometrically necessary dislocations (GND), that is, dislocations that must be present near the indentation to accommodate the volume of material displaced by the indenter at the surface, along with the usual statistically stored dislocations (SSD) produced during uniform straining. The addition of this extra component becomes larger as the contact between indenter and material decreases in size, producing the aforementioned effect [72].

As it was commented before, the indentation size effect, ISE, in EUROFER97 and EU-ODS EUROFER steel in as-received state was already studied and published elsewhere [19,34]. In these works, H^2 vs. 1/h curves from 500 nm up to 150 nm aproximately were graphed for both steels. In which it was described how, when applying Nix and Gao model, it was observed that both materials showed a trend characterized by 3 zones. The first one, fits the Nix and Gao model from about 500 nm depth to beyond, and turns out that is practically the same value for both materials. This zone would represent the microindentation hardness tests. Then, another linear zone, after a transition zone, begins at a different depth depending on the material, which was called zone 2. However, for the actual research, shallower depths than 150 nm for as-received steels must be evaluated to be able to compare all H^2 vs. 1/h curves after being irradiated with He at different temperatures . The linear behavior is the one repreenting zone 2 mentioned in [19], because the depths are much shallower than the zone 1 that is needed to studied Nix and Gao model. After testing, Fig. 17a-b) for EUROFER97 and EU-ODS EUROFER respectively were built. It was observed that the curve representing the as-received state of EUROFER97 from about 240 nm in depth and 330 nm approximately for EU-ODS EUROFER showed a linear behavior up to approximately 22 nm and 30 nm respectively. Compared with the other curves, it is noted that depth where the linear behavior changes increases with irradiation temperature, making parabolic so the ending of the zone 2 shifts to larger depths in both materials. It draws attention the behavior of steel EUROFER97 implanted at 350 °C, which does not follow the same trend as other experiments and it presents more linear behavior, as well as slight oscillations which were also recorded in the results of the irradiations at RT and 450 °C respectively, which are probably due to a poorer statistic, since the plotted curves are obtained from the average of the valid indentations for each experiment. On the other hand, for EU-ODS EUROFER the results were very similar, being the most characteristic similarity between the results in as received state and the implantation at room temperature. Nevertheless, the change in depth of the zone 2 along with the increase in hardness values, may represent a combination of the accumulation of irradiation defects with an enhance indentation size effect in those materials.

For irradiated steels some authors have developed a method that evaluates the increase in hardness as a function of irradiation damage or dpa [73,74]. This approach is based on Gao and Nix model but extended to a multilayer material system. In this method, the final part of the curve (which coincides with the first nanometers in depth) where it is assumed that the effect of irradiation in the hardness is larger, is analyzed making a difference with deeper indentations. However, the major problem with this method is that the authors who applied it [75–78] analyzed up to about 100 nm (10 μm^{-1}) in depth even for shallow irradiations, missing information, because, on one hand, it is considering that the plastification volume affects 3 to 4 times the indentation depth, so if the first 50 to 100 nm are removed or not taken into consideration, so a part of the interaction between the indentation and the implanted material in the first 300 or 400 nm is being neglected. For irradiations of He at 40 keV, whose maximum concentration of damage is located at approximately at 150 nm, it was observed that from practically the very surface many cavities were detected (depending on the irradiation temperature). Therefore, it is not valid to use this simplification, and it is necessary to start analyzing from almost 20 nm (or less if the resolution of the device makes it possible) with the

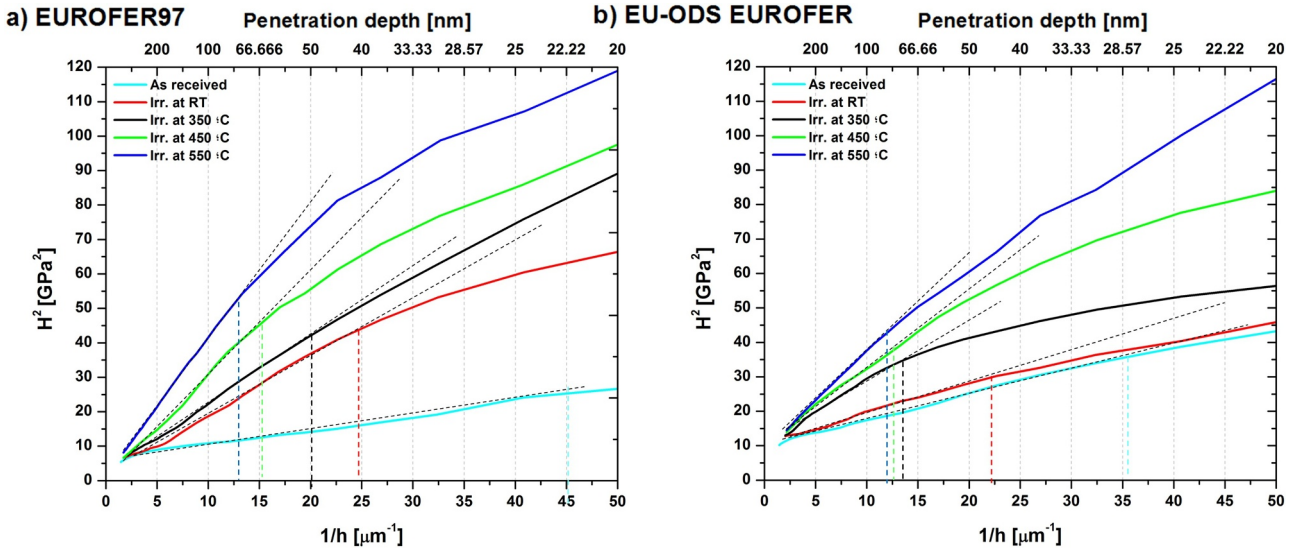

Fig. 17. H^2 vs. 1/h curves of (a) EUROFER97 and (b) EU-ODS EUROFER indicating the depth where the linear behavior changes.

interpretation difficulties inherent to deal with very shallowing mechanics. It can be checked in Fig. 17 from 20 to 100 nm for both steels that the curves are no longer linear showing evidence that possibly the accumulation of defects due to irradiation is altering the way the material accommodates the defects produced by the indenting.

For other kind of experiments, where the irradiation damage peak is located deeper, as irradiation with protons [34] or even when the hardness vs. indentation depth curves show a significant slope change because the material has been damaged at higher doses [74–80], it is possible to make that simplification. One material irradiated with He has a very different response than to being irradiated with ions of a different nature such as Xe [75] producing different curves hardness vs. displacement, for which analysis must be done with special considerations regarding the irradiation characteristics.

The Nix and Gao model was formulated for homogeneous materials with isotropic mechanical properties, since the material does not have these, the accommodation of dislocations mechanisms may be very different. It is required to go deeper into this field to establish a model that eliminates the effect of the indentation size in the surface modified materials by irradiation. However, so far, to perform a semi quantitative comparison, the H_{IRR} / H_{UNIRR} ratio seems to be the best way to analyze the effects of shallow irradiation (for both light and heavy ions).

Generally speaking, it has been experimentally demonstrated that structural materials candidates for the future fusion reactor, EUROFER97 and EU-ODS EUROFER, showed what is known as radiation induced hardening. This increase in hardness values is caused by the defects created during irradiation (such as cavities and dislocations among others), which will depend on the experimental conditions such as radiant species nature, irradiation temperature or fluence. It has been shown that both loops dislocation as cavities are major obstacles which act as barriers to movement of dislocations, resulting in an increase of hardness values of the irradiated materials, but so are other microstructural characteristics (irradiation independent) such as grain boundaries, dislocations inherent to the microstructure, precipitated or added particles as yttrium oxides (in the case of ODS). In order to correlate microstructural defects with the increase in hardness in a theoretical manner, some authors have used the model known as dispersed barrier hardening [81,82] applied to defect sizes and densities for both experimentally measured and simulated results. Recalling the results obtained by nanoindentation from the He implanted at room temperature EUROFER97 and EU-ODS EUROFER published elsewhere [19], noted how the former showed a greater increase in hardness values of 41% compared with the second steel, in which the maximum increase in hardness value was 21%. This behavior was observed again in this research, even when both the experimental conditions of implantation as nanomechanical analysis mode changed (continuous stiffness measurements vs. quasi-static mode) confirming the robustness of the experimental procedure. Analyzing Fig. 16 it is possible to observe that the increase in hardness of EU-ODS EUROFER is much lower compared to the EUROFER97. Indeed, taking the maximum values around the transition line, the increase in hardness can be calculated, and provided with caution considering that the effect of the indentation size is present and the results would have a semi quantitative value. For EUROFER97, Fig. 6a, an increase of 67% was measured while for EU-ODS EUROFER, Fig. 6b, it was around of 5.5%. Comparing the microstructure of both materials, presented above, it was observed that the population of cavities was the same order of magnitude in both steels up to 450 °C, when it experiences an increase in EU-ODS EUROFER to show a large decrease at 550 °C. Moreover, the total amount of generation of defects (in terms of vacancies and interstitials) was higher when the specimens were implanted with stair-like profile (MeV) [19,34] than for this irradiation at 40 keV, so it is likely that factor is one to be taken into consideration. Clearly, the way EU-ODS EUROFER accommodate defects when irradiated He at room temperature is better that of EUROFER97, since the increase in hardness is less pronounced. A similar behavior has been observed by Yang et al. [43] where an ODS steel, MA956, was compared to a ferritic martensitic steel, T92, both irradiated with He at room temperature with a similar fluence and ion energy to the ones used in these experiment. The results showed that the increase in hardness is less for the ODS than for the ferritic-martensitic steel, in spite of the fact that the composition of MA956 differs from the EU-ODS EUROFER. Furthermore, it was detected by nanoindentation analogously to the results obtained and presented here a maximum hardness peak at a depth of about 1/3 to 1/4 times the maximum implantation depth, which corroborates the effect of inhibiting defects produced by irradiating He at room temperature. Some other studies were performed in similar materials, obtaining values of cavity diameter and population density in the same order of magnitud. Nevertheles, it must be taken into conisderation that the experimental conditions were no completely the same, and the way of measuring these parameters may difer. Lu et al. [83] implanted samples of 14Cr-ODS and EUROFER97 with 1×10^{17} He/cm^2 at 400 °C. They observed much larger cavities even up 28 nm, and the behavior of coalescence is different, the ODS samples reduce the growth of cavities. However, these bservations can be explained because the implantation depth was more significant and hence, the material has more amount of possible sinks that may act as defect annihilators. Li et al. [84] implanted He at 6.75×10^{20} He/m2 and 400 °C, measuring a population sensity of 8.4×10^{23} m^{-3} at the peak with a diameter similar to the one measured in this research. However, the irradiation conditions are different since the dose is much larger. Edmonson et al. [46] irradiated He at 6.75×10^{20} and 400 °C with 335 keV He observing 2×10^{23} m^{-3}. Even for neutron irradiated specimens with the production of He by transmutation, the values are similar: Odette et al. [85] irradiated some samples of nanostructured ferritic alloys up to 380 appm He with 4.8 MeV He. They calculated a density of $74{,}3 \times 10^{23}$ m^{-3} for MA95 and 5.3×10^{22} m^{-3} for TMS F82H. Regarding, diameters the cavities showed average size of arounf 2 nm. Finally, Yamamoto et al. [86] studied a variation of F82H irradiated at HFIR at 500 °C, 9 dpa and 190 and 380 appm He. The maximum frequency of cavity diameter observed was of around 2 nm and the density 5.3×10^{22} m^{-3}. However, as the temperature increased it seems that this effect decreases, since EU-ODS EUROFER shows an increase in hardness values, possibly due to nucleation and/or growth of new cavities. In fact, correlating the microstructural observations with the nanoindentation results, it was observed that as the temperature increases EU-ODS EUROFER steel presented larger cavities with a more heterogeneous distribution, unlike EUROFER97 which seems to have smaller ones distributed in an aligned manner throughout the matrix acting as barriers to dislocations. This change in the way the cavities nucleated and diffused towards defects sinks suggests different mechanisms inherent to the microstructure.

Another result to note is that in both EUROFER97 and EU-ODS EUROFER all the nanoindentation curves, regardless of the temperature at which the specimens have been irradiated, converge towards a certain hardness value (which is the hardness of the as received state) at a penetration depth around 400–500 nm. This behavior confirms the effect of softer substrate, where the influence of the unirradiated material volume analyzed is so large in comparison with the implanted one that it inhibits the effects of the irradiation defects [45]. With other experimental conditions, where deeper irradiations were performed using other methodologies such as beam degraders or sequential irradiations in order to obtain homogeneous and flat profiles, this phenomenon is equally observed. Curves do not converge until the penetration depth is much greater than the implantation depth, taking into account the ratio indentation volume (which is the volume occupied by the nanoindentation tip) and plastification volume [65,87,88]. In regard to the exact value of hardness value as depth increases, further

analysis can be done, instead of a comparative study as presented here. A new model to analyze ion irradiated specimens has been proposed [89].

5. Conclusions

The most remarkable conclusions extracted from this research are as follows:

- Nanoindentation testing mode continuous stiffness measurement was used to analyze the normal surface to the irradiation beam of EUROFER97 and EU-ODS EUROFER steels implanted with He at room temperature, 350 °C, 450 °C and 550 °C. A clear increase of the hardness values in the first 500 nm is observed, the higher the irradiation temperature, the higher the effect.
- The increase in nanoindentation hardness values compared to the as received state is higher in the steel EUROFER97 than the EU-ODS EUROFER. Both steels showing an absolute maximum when the irradiation temperature was 550 °C.
- Nix and Gao model was applied to the implanted materials at different temperatures, noting a more pronounced curved profile than for the material in the as received state. The deviation of the results with the theoretical model would require a systematic microstructural analysis of dislocations generated by the indentation and the defects produced by He irradiation in order to perform a further correlation between microstructure and hardness results. This research was outside the scope of this paper.
- Both materials experienced a population increase of nanocavities as the implantation temperature increased, reaching a maximum at 450 °C.
- EUROFER97 presented aligned cavities at 450 °C and 550 °C, that they were nucleated in grain or sub grain boundaries and/or even dislocations.
- EU-ODS EUROFER did not show such an alignment. However, it was detected a very significant increase in cavity population at 450 °C, and at 550 °C a general increase in the cavity size at the expense of a decrease of the population was detected. This suggests that the mechanism of nucleation, growth and fate of the cavities is clearly different between 450 °C and 550 °C and it is strongly microstructure dependent.

Acknowledgments

The authors want to thank the National centre from Electronic Microscopy (CNME) staff and all the researchers and technicians from CIEMAT (especially F. Mota and C. Ortiz, for their calculus and support), Rey Juan Carlos University and CMAM (Centro de Microanálisis de Materiales) are also acknowledged for providing help and equipment. This work has been supported by Ministerio de Ciencia, Innovación y Universidades Projects: ENE2015-70300-C3-1-R and MAT2012-384407-C03-01, Techno Fusion Project (S2018/EMT4437) of the CAM (Comunidad Autónoma Madrid) and partially by The European Regional Development Fund and in particular, the Operational Programme for R + D + i (Technology Fund) and the European Communities within the European Fusion Technology Programme 2014–2018 under agreement No 633053. “The views and opinions expressed herein do not necessarily reflect those of the European Commission”. The authors want to acknowledge Natalia Willey Toledo for her help with language editing, improving the paper quality.

References

[1] D. Stork, et al., Developing structural, high-heat flux and plasma facing materials for a near-term DEMO fusion power plant: the EU assessment, J. Nucl. Mater. 455 (1–3) (2014) 277–291.
[2] S.J. Zinkle, A. Möslang, Evaluation of irradiation facility options for fusion materials research and development, Fusion Eng. Des. 88 (6–8) (2013) 472–482.
[3] J. Knaster, A. Moeslang, T. Muroga, Materials research for fusion, Nat. Phys. (2016) 424–434.
[4] S.J. Zinkle, G.S. Was, Materials challenges in nuclear energy, Acta Mater. 61 (3) (2013) 735–758.
[5] S.J. Zinkle, L.L. Snead, Designing radiation resistance in materials for fusion energy, Annu. Rev. Mater. Res. 44 (1) (2014) 241–267.
[6] R. Lindau, et al., Mechanical and microstructural properties of a hipped RAFM ODS-steel, J. Nucl. Mater. 307–311 (Part 1(0)) (2002) 769–772.
[7] S. Ukai, M. Fujiwara, Perspective of ODS alloys application in nuclear environments, J. Nucl. Mater. 307–311 (Part 1) (2002) 749–757.
[8] G.R. Odette, M.J. Alinger, B.D. Wirth, Recent developments in irradiation-resistant steels, Annu. Rev. Mater. Res. 38 (1) (2008) 471–503.
[9] J. Brodrick, D.J. Hepburn, G.J. Ackland, Mechanism for radiation damage resistance in yttrium oxide dispersion strengthened steels, J. Nucl. Mater. 445 (1–3) (2014) 291–297.
[10] C. Heintze, et al., The influence of helium and ODS on the irradiation-induced hardening of EUROFER97 at 300°C, Adv. Sci. Technol. (2010).
[11] Lu, C., et al., Enhanced radiation-tolerant oxide dispersion strengthened steel and its microstructure evolution under helium-implantation and heavy-ion irradiation. 2017.7: p. 40343.
[12] C. Dethloff, Modeling of Helium Bubble Nucleation and Growth in Neutron Irradiated RAFM Steels, KIT, 2012.
[13] H. Trinkaus, B.N. Singh, Helium accumulation in metals during irradiation – where do we stand? J. Nucl. Mater. 323 (2–3) (2003) 229–242.
[14] A.A.F. Tavassoli, et al., Current status and recent research achievements in ferritic/martensitic steels, J. Nucl. Mater. 455 (1–3) (2014) 269–276.
[15] D. Stork, et al., Materials R&D for a timely DEMO: key findings and recommendations of the EU roadmap materials assessment group, Fusion Eng. Des. 89 (7–8) (2014) 1586–1594.
[16] Y. Katoh, et al., The influence of He/DPA ratio and displacement rate on microstructural evolution: a comparison of theory and experiment, J. Nucl. Mater. 210 (3) (1994) 290–302.
[17] H. Trinkaus, The effect of cascade induced gas resolution on bubble formation in metals, J. Nucl. Mater. 318 (0) (2003) 234–240.
[18] C.A. Williams, et al., Nanoscale characterisation of ODS–Eurofer 97 steel: an atom-probe tomography study, J. Nucl. Mater. 400 (1) (2010) 37–45.
[19] M. Roldán, et al., Comparative study of helium effects on EU-ODS EUROFER and EUROFER97 by nanoindentation and TEM, J. Nucl. Mater. 460 (0) (2015) 226–234.
[20] P. Fernández, et al., RAFM Steel eurofer'97 As Possible Structural Material For Fusion device. Metallurgical characterization On As Received Condition and After Simulated Service Conditions, Inorme técnico CIEMAT, 2004.
[21] H.R.Z. Sandim, et al., Annealing behavior of ferritic–martensitic 9%Cr–ODS–Eurofer steel, Mater. Sci. Eng. A 527 (15) (2010) 3602–3608.
[22] R. Lindau, et al., Present development status of EUROFER and ODS-EUROFER for application in blanket concepts, Fusion Eng. Des. 75–79 (2005) 8.
[23] M.T. Robinson, I.M. Torrens, Computer simulation of atomic-displacement cascades in solids in the binary-collision approximation, Phys. Rev. B 9 (12) (1974) 5008–5024.
[24] M.T. Robinson, Slowing-down time of energetic atoms in solids, Phys. Rev. B 40 (16) (1989) 10717–10726.
[25] J. Krier, et al., Introduction of the real tip defect of Berkovich indenter to reproduce with FEM nanoindentation test at shallow penetration depth, J. Mater. Res. 27 (1) (2012) 28–38.
[26] S. Chen, F. Ke, MD simulation of the effect of contact area and tip radius on nanoindentation, Sci. China Ser. G 47 (1) (2004) 101–112.
[27] Agilent, Manual nanoindenter XP MTS Testworks 4. 2002.
[28] L.A. Giannuzzi, et al., Theory and new applications of ex situ lift out, Microsc. Microanal. 21 (4) (2015) 1034–1048.
[29] L.A. Giannuzzi, F.A. Stevie, A review of focused ion beam milling techniques for TEM specimen preparation, Micron 30 (3) (1999) 197–204.
[30] N.I. Kato, Reducing focused ion beam damage to transmission electron microscopy samples, J. Electron. Microsc. 53 (5) (2004) 451–458.
[31] J. Mayer, et al., TEM sample preparation and FIB-Induced damage, MRS Bull. 32 (5) (2007) 400–407.
[32] M. Roldán, et al., The effect of triple ion beam irradiation on cavity formation on pure EFDA iron, J. Nucl. Mater. 479 (2016) 100–111.
[33] R.E. Dunin-Borkowski, The development of FRESNEL contrast analysis, and the interpretation of mean inner potential profiles at interfaces, Ultramicroscopy 83 (3–4) (2000) 193–216.
[34] M. Roldán, et al., Effect of helium implantation on mechanical properties of EUROFER97 evaluated by nanoindentation, J. Nucl. Mater. 448 (1–3) (2014) 301–309.
[35] B. Yao, et al., Multislice simulation of transmission electron microscopy imaging of helium bubbles in Fe, J. Electron. Microsc. (2012).
[36] M.L. Jenkins, M.A. Kirk, Characterization of Radiation Damage by TEM, Institute of physics, 2001.
[37] D. Hull, D.J. Bacon, Introduction to Dislocations, 5. ed ed, Elsevier/Butterworth-Heinemann, Amsterdam, 2011, p. 257.
[38] M. Klimenkov, A. Möslang, E. Materna-Morris, Helium influence on the microstructure and swelling of 9%Cr ferritic steel after neutron irradiation to 16.3dpa, J. Nucl. Mater. 453 (1–3) (2014) 54–59.
[39] M. Klimenkov, et al., Helium bubble morphology of boron alloyed EUROFER97 after neutron irradiation, J. Nucl. Mater. 442 (1–3, Supplement 1) (2013) S52–S57.
[40] V. Krsjak, et al., Helium behavior in ferritic/martensitic steels irradiated in

spallation target, J. Nucl. Mater. 456 (0) (2015) 382–388.
[41] H. Trinkaus, Energetics and formation kinetics of helium bubbles in metals, Radiat. Eff. 78 (1–4) (1983) 189–211.
[42] B.N. Singh, H. Trinkaus, An analysis of the bubble formation behaviour under different experimental conditions, J. Nucl. Mater. 186 (2) (1992) 153–165.
[43] Y. Yang, et al., Nanoindentation on an oxide dispersion strengthened steel and a ferritic/martensitic steel implanted with He ions, J. Nucl. Mater. 455 (1–3) (2014) 325–329.
[44] M.J. Aliaga, M.J. Caturla, R. Schäublin, Surface damage in TEM thick α-Fe samples by implantation with 150keV Fe ions, Nucl. Instrum. Methods Phys. Res. Sect. B 352 (2015) 217–220.
[45] M.J. Aliaga, et al., Surface-induced vacancy loops and damage dispersion in irradiated Fe thin films, Acta Mater. 101 (2015) 22–30.
[46] P.D. Edmondson, et al., Helium bubble distributions in a nanostructured ferritic alloy, J. Nucl. Mater. 434 (1–3) (2013) 210–216.
[47] M.L. Jenkins, M.A. Kirk, W.J. Phythian, Experimental studies of cascade phenomena in metals, J. Nucl. Mater. 205 (1993) 16–30.
[48] D.J. Bacon, F. Gao, Y.N. Osetsky, The primary damage state in fcc, bcc and hcp metals as seen in molecular dynamics simulations, J. Nucl. Mater. 276 (1–3) (2000) 1–12.
[49] Y.N. Osetsky, et al., Stability and mobility of defect clusters and dislocation loops in metals, J. Nucl Mater. 276 (1–3) (2000) 65–77.
[50] Zinkle, S.J.Microstructure and mechanical properties of irradiated metals and alloys. Chapter of book. Materials Issues for Generation IV systems, ISBN 978-1-4020-8423-2, p 227–244.
[51] G.R. Odette, Recent progress in developing and qualifying nanostructured ferritic alloys for advanced fission and fusion applications, JOM 66 (12) (2014) 2427–2441.
[52] A.I. Ryazanov, et al., Tensile properties and microstructure of helium implanted EUROFER ODS, J. Nucl. Mater. 442 (1, Supplement 1) (2013) S153–S157.
[53] F. Luo, et al., Damage behavior in helium-irradiated reduced-activation martensitic steels at elevated temperatures, J. Nucl. Mater. 455 (1–3) (2014) 339–342.
[54] T.R. Allen, et al., The effect of dose rate on the response of austenitic stainless steels to neutron radiation, J. Nucl. Mater. 348 (1–2) (2006) 148–164.
[55] T. Okita, et al., The primary origin of dose rate effects on microstructural evolution of austenitic alloys during neutron irradiation, J. Nucl. Mater. 307–311 (Part 1) (2002) 322–326.
[56] C.D. Hardie, et al., Effects of irradiation temperature and dose rate on the mechanical properties of self-ion implanted Fe and Fe–Cr alloys, J. Nucl. Mater. 439 (1–3) (2013) 33–40.
[57] G.S. Was, Fundamentals of Radiation Materials Science (metals and Alloys), Springer, 2007.
[58] Y. Ortega, et al., Void formation in ods eurofer produced by hot isostatic pressing, J. Nucl. Mater. 386–388 (0) (2009) 462–465.
[59] D. Kiener, et al., Application of small-scale testing for investigation of ion-beam-irradiated materials, J. Mater. Res. 27 (21) (2012) 2724–2736.
[60] P. Hosemann, et al., Issues to consider using nano indentation on shallow ion beam irradiated materials, J. Nucl. Mater. 425 (1–3) (2012) 136–139.
[61] Q. Ma, D.R. Clarke, Size dependent hardness of silver single crystals, J. Mater. Res. 10 (4) (1995) 853–863.
[62] H. Li, A.H.W. Ngan, Size effects of nanoindentation creep, J. Mater. Res. 19 (2) (2004) 513–522.
[63] D. Kiener, et al., Microstructural evolution of the deformed volume beneath microindents in tungsten and copper, Acta Mater. 54 (10) (2006) 2801–2811.
[64] S.J. Lloyd, et al., Observations of nanoindents via cross-sectional transmission electron microscopy: a survey of deformation mechanisms, Proc. R. Soc. London A 461 (2060) (2005) 2521–2543.
[65] K.K. McLaughlin, W.J. Clegg, Deformation underneath low-load indentations in copper, J. Phys. D 41 (7) (2008) 074007.
[66] C.D. Hardie, S.G. Roberts, Nanoindentation of model Fe–Cr alloys with self-ion irradiation, J. Nucl. Mater. 433 (1–3) (2013) 174–179.
[67] H. Tanigawa, et al., Effects of helium implantation on hardness of pure iron and a reduced activation ferritic - martensitic steel, J. Nucl. Mater. (2000) 4.
[68] I. Manika, J. Maniks, Effect of substrate hardness and film structure on indentation depth criteria for film hardness testing, J. Phys. D 41 (7) (2008) 074010.
[69] R. Saha, W.D. Nix, Effects of the substrate on the determination of thin film mechanical properties by nanoindentation, Acta Mater. 50 (1) (2002) 23–38.
[70] T.Y. Tsui, G.M. Pharr, Substrate effects on nanoindentation mechanical property measurement of soft films on hard substrates, J. Mater. Res. 14 (1) (1999) 292–301.
[71] W.D. Nix, H. Gao, Indentation size effects in crystalline materials: a law for strain gradient plasticity, J. Mech. Phys. Solids 46 (3) (1998) 411–425.
[72] Y.V. Milman, A. Golubenko, S.N. Dub, Indentation size effect in nanohardness, Acta Mater. 59 (20) (2011) 7480–7487.
[73] Y. Takayama, et al., Evaluation of irradiation hardening of Fe-ion irradiated F82H by nano-indentation techniques, Mater. Sci. Forum 654–656 (2010) 4.
[74] R. Kasada, et al., A new approach to evaluate irradiation hardening of ion-irradiated ferritic alloys by nano-indentation techniques, Fusion Eng. Des. 86 (9–11) (2011) 2658–2661.
[75] H. Zhang, et al., Irradiation hardening of ODS ferritic steels under helium implantation and heavy-ion irradiation, J. Nucl. Mater. 455 (1–3) (2014) 349–353.
[76] X. Liu, et al., Evaluation of radiation hardening in ion-irradiated Fe based alloys by nanoindentation, J. Nucl. Mater. 444 (1–3) (2014) 1–6.
[77] Y. Yang, et al., Nanoindentation on V–4Ti alloy irradiated by H and He ions, J. Nucl. Mater. 459 (0) (2015) 1–4.
[78] P. Hosemann, et al., Macro and microscale mechanical testing and local electrode atom probe measurements of STIP irradiated F82H, Fe–8Cr ODS and Fe–8Cr–2W ODS, J. Nucl. Mater. 417 (1–3) (2011) 274–278.
[79] Y. Takayama, et al., Nanoindentation hardness and its extrapolation to bulk-equivalent hardness of F82H steels after single- and dual-ion beam irradiation, J. Nucl. Mater. 442 (1–3, Supplement 1) (2013) S23–S27.
[80] K. Yabuuchi, R. Kasada, A. Kimura, Effect of alloying elements on irradiation hardening behavior and microstructure evolution in BCC Fe, J. Nucl. Mater. 442 (1–3, Supplement 1) (2013) S790–S795.
[81] G.E. Lucas, The evolution of mechanical property change in irradiated austenitic stainless steels, J. Nucl. Mater. 206 (2–3) (1993) 287–305.
[82] J. Gan, G.S. Was, Microstructure evolution in austenitic Fe–Cr–Ni alloys irradiated with rotons: comparison with neutron-irradiated microstructures, J. Nucl. Mater. 297 (2) (2001) 161–175.
[83] C. Lu, et al., Microstructure of a 14Cr-ODS ferritic steel before and after helium ion implantation, J. Nucl. Mater. 455 (1–3) (2014) 366–370.
[84] Q. Li, et al., Helium solubility and bubble formation in a nanostructured ferritic alloy, J. Nucl. Mater. 445 (1–3) (2014) 165–174.
[85] G.R. Odette, et al., Helium transport, fate and management in nanostructured ferritic alloys: in situ helium implanter studies, J. Nucl. Mater. 417 (1–3) (2011) 1001–1004.
[86] T. Yamamoto, et al., Helium effects on microstructural evolution in tempered martensitic steels: in situ helium implanter studies in HFIR, J. Nucl. Mater. 386–388 (2009) 338–341.
[87] E.M. Grieveson, S.G. Roberts, Investigation into irradiation effects in ODS steels using ion implantation and micromechanical testing, Fusion Engineering (SOFE), 2013 IEEE 25th Symposium on, 2013.
[88] R. Kasada, et al., Depth-dependent nanoindentation hardness of reduced-activation ferritic steels after MEV Fe-ion irradiation, Fusion Eng. Des. (0) (2014).
[89] X. Xiao, et al., A mechanistic model for depth-dependent hardness of ion irradiated metals, J. Nucl. Mater. 485 (2017) 80–89.